Characterization of swift heavy ion tracks in MoS_2 by transmission electron microscopy*

Li-Jun Xu(徐丽君)[1,2], Peng-Fei Zhai(翟鹏飞)[1,2,†], Sheng-Xia Zhang(张胜霞)[1], Jian Zeng(曾健)[1,2], Pei-Pei Hu(胡培培)[1], Zong-Zhen Li(李宗臻)[1,2], Li Liu(刘丽)[1,2], You-Mei Sun(孙友梅)[1,2], and Jie Liu(刘杰)[1,2,‡]

[1] *Institute of Modern Physics, Chinese Academy of Sciences, Lanzhou* 730000, *China*

[2] *School of Nuclear Science and Technology, University of Chinese Academy of Sciences, Beijing* 100049, *China*

(Received 27 April 2020; revised manuscript received 6 August 2020; accepted manuscript online 7 August 2020)

The various morphologies of tracks in MoS_2 irradiated by swift heavy ions at normal and 30° incidence with 9.5–25.0 MeV/u ^{86}Kr, ^{129}Xe, ^{181}Ta, and ^{209}Bi ions were investigated by transmission electron microscopy. The diameter of ion tracks increases from 1.9 nm to 4.5 nm with increasing electronic energy loss. The energy loss threshold of the track formation in MoS_2 is predicted as about 9.7 keV/nm based on the thermal spike model and it seems consistent with the experimental results. It is shown that the morphology of ion tracks is related to the penetration length of ions in MoS_2. The formation process of ion tracks is discussed based on the cooperative process of outflow and recrystallization of the molten phase during rapid quenching.

Keywords: ion track, MoS_2, transmission electron microscopy (TEM), recrystallization

PACS: 61.80.–x, 61.82.–d, 68.37.Lp **DOI:** 10.1088/1674-1056/abad1e

1. Introduction

Swift heavy ions (SHIs) with specific energy more than 1 MeV/u deposit their energy into the target electrons predominately by ionization and electronic excitation (i.e., electronic energy loss) during slowing down in solids. After transferring the deposited energy to the target lattice by electron–phonon coupling,[1] a permanent damage along the ion path, so called ion track or latent track, can be produced. Usually, the ion track is cylindrical with several nanometers in diameter. SHIs can be used to modify the material properties by controlling the incident energy and radiation fluence. Recently, many potential applications of SHIs have been demonstrated, such as the nano-filtration membranes,[2,3] nanopores for single biomolecular detection,[4] and ion track templates for electronic devices.[5] Therefore, SHIs irradiation is considered to be one of the most powerful tools for defect engineering at the atomic scale in materials.[6–11]

Molybdenum disulfide (MoS_2) has attracted much attention due to its outstanding electrical, mechanical, and optical properties.[12–15] As a typical layered material, it can be exfoliated to monolayer or a fewer layers because of the weak Van der Waals force between layers. In particular, MoS_2 can be transferred from indirect to direct band-gap material when its thickness decreases to single layer. Moreover, a single layer MoS_2 transistor was found with ultrahigh mobility and current on/off ratio at room temperature.[12]

Ion irradiations in MoS_2 can introduce nano-defect structure and thereby change the physical, catalytic, or electronic performance. Madauß *et al.*[11] observed the nano-hillocks, foldings, and nano-incisions in irradiated MoS_2 with the thickness ranging from bulk down to single layer by atomic force microscopy (AFM). However, due to the limited resolution and finite curvature radius of the AFM tip, the actual size and structure inside the bulk cannot be obtained by this technique. On the other hand, despite the craters, bumps, and onion-like structures were observed in MoS_2 irradiated with cluster ions C_{60},[16] the electronic energy loss $(\mathrm{d}E/\mathrm{d}x)_e$ of the cluster ions was much higher than that of GeV monoatomic heavy ions. Until now, the detailed morphology and structure of ion tracks in MoS_2 irradiated with GeV heavy ions have not been illustrated and the formation process and mechanism are still unclear. More recently, we reported that the morphology of ion track in rutile TiO_2 evolves as a function of ion path length from cylinder to dumbbell-shape and then to sandglass-shape.[17] To the best of our knowledge, the conical track near the surface of the sample was observed only in several metal oxides, such as rutile TiO_2,[17] Al_2O_3,[18] yttria-stabilized cubic ZrO_2 (YSZ),[19] and $Gd_2Zr_2O_7$ pyrochlore.[20] Further work is required to thoroughly explore the interpretation of the conical track formation in some materials.

In this work, we report the direct observations of the various morphologies of tracks in irradiated MoS_2 with the help of transmission electron microscopy (TEM). Furthermore, we reveal that the morphology of ion tracks in MoS_2 is dependent on the ion path length. Based on the experimental evidence, the outflow of molten phase and recrystallization during rapid

*Project supported by the National Natural Science Foundation of China (Grant Nos. 11675233, 11690041, 11405229, 11705246, and 11505243), Chinese Academy of Sciences "Light of West China" Program, and the Youth Innovation Promotion Association of Chinese Academy of Sciences (Grant No. 2020412).

†Corresponding author. E-mail: zhaipengfei@impcas.ac.cn

‡Corresponding author. E-mail: j.liu@impcas.ac.cn

quenching are proposed to explain the formation mechanism of various morphologies of ion tracks in MoS_2.

2. Experimental details

The fine powders of MoS_2 with sample size 200 nm–2 μm were supplied by Goodfellow Corporation, its thickness was around 30–200 nm. After ultrasonic treatment for the MoS_2 powders mixed with ethanol, the samples were dispersed on TEM copper grids, which were directly used for irradiation experiments and TEM observation. The schematic diagram is shown in Fig. 1. Irradiation experiments were performed in Heavy Ion Research Facility in Lanzhou (HIRFL). The samples were irradiated by ^{86}Kr, ^{129}Xe, ^{181}Ta, and ^{209}Bi ions with initial kinetic energies of 25.0 MeV/u, 19.5 MeV/u, 12.5 MeV/u, and 9.5 MeV/u under normal incidence, respectively. Some samples were irradiated by ^{181}Ta ions with initial kinetic energy of 1785.7 MeV at 30° oblique angle (relative to normal direction) at room temperature. The range of ion fluence was chosen between 5×10^{10} ions/cm^2 and 5×10^{12} ions/cm^2 in order to easily find and observe the tracks in TEM. The ion flux was detected on-line by the 18 μm aluminum foils detector which was less than 2×10^8 ions/(cm^2·s) to avoid macroscopic heating in the samples. The fluence was determined with an uncertainty of 10%–20%. Aluminum degraders (99.99% purity) with different thicknesses were usually placed in front of the samples in order to change the incident energy. The specific irradiation parameters of MoS_2 calculated by SRIM-2013 are displayed in Table 1. As the $(dE/dx)_e$ is three orders of magnitude larger than the nuclear energy loss $(dE/dx)_n$, the influence of the nuclear energy loss can be neglected. The irradiated samples were characterized by TEM (FEI Tecnai G2 F20 S-TWIN) with 200 kV accelerating voltages. To determine the average ion track diameter (D_a), more than 100 ion tracks were measured for each irradiated sample using the free software Nano Measurer.

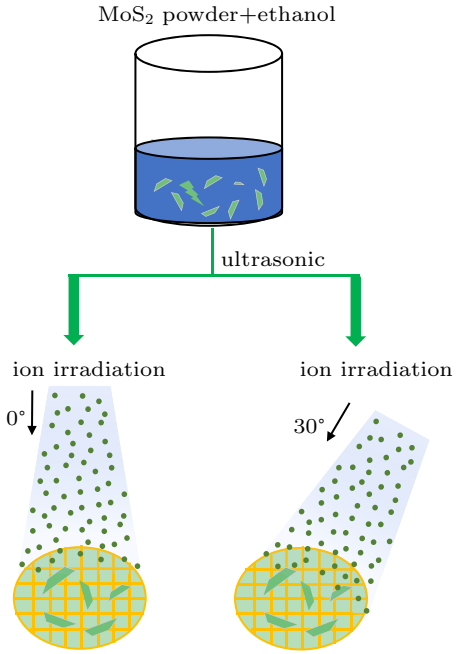

Fig. 1. A sketch map of experiment process.

Table 1. Irradiation parameters for MoS_2.

Ion	Energy/MeV	$(dE/dx)_e$/(keV/nm)	$(dE/dx)_n$/(keV/nm)	Range/μm	Fluence/(ions/cm^2)
^{86}Kr	2029.4	7.7	3.9×10^{-3}	193.6	5×10^{10}
^{86}Kr	1795.3	8.2	4.4×10^{-3}	164.0	5×10^{10}
^{86}Kr	1503.4	9.1	5.1×10^{-3}	130.2	5×10^{10}
^{129}Xe	2047.5	18.9	1.2×10^{-2}	96.8	5×10^{12}
^{181}Ta	1785.7	28.8	3.2×10^{-2}	65.8	5×10^{10}
^{209}Bi	1390.0	35.2	5.7×10^{-2}	46.8	5×10^{11}

3. Results and discussion

Figure 2 shows the plan-view TEM images of the irradiated MoS_2 with Xe, Ta, and Bi ions. A number of tracks were observed after Xe, Ta, and Bi ions irradiation and it was found that the number of tracks increases with increasing ion fluence. The left and right TEM images of the same area were taken under the over-focus and under-focus conditions, respectively. The different contrasts of the tracks can be seen clearly. Such Fresnel contrast indicates that the lower density or empty region than the matrix was formed along the ion path.[17,21,22] According to the projection charge density approximation, the intensity distribution of image in TEM is given by[23]

$$I(x,y) = 1 + 2l\sigma\lambda\rho(x,y), \quad (1)$$

where l is the distance from the image plane, σ is interaction constants, λ is the defocus distance, and $\rho(x,y)$ is the projected charge distribution. The projected charge distribution of light elements or low density areas is small, and the phase contrast reversal will occur when $\lambda > 0$ or $\lambda < 0$.

No tracks were observed after Kr ions irradiation, the $(dE/dx)_e$ of which are 7.7 keV/nm, 8.2 keV/nm, and 9.1 keV/nm, respectively. Therefore, the electronic energy loss threshold for the formation of tracks in MoS_2 induced by ∼ 15 MeV/u heavy ions should fall between 9.1 keV/nm (1503.4 MeV Kr) and 18.9 keV/nm (2047.5 MeV Xe). Moreover, Szenes *et al.* proposed the following formula which could quantitatively predict the energy loss threshold (S_{et}) of

the track formation:[24]

$$S_{\rm et} = \pi\rho c T_0 a^2(0)/g, \tag{2}$$

where ρ, c, and T_0 denote the density, the average specific heat, and the difference between the melting point $T_{\rm m}$ and the irradiation temperature $T_{\rm ir}$, respectively. For MoS_2, ρ is 4.8 g/cm^3, c is 0.5 J/g·K,[25] and $T_0 = T_{\rm m} - T_{\rm ir} = 1723$ K, where $T_{\rm ir}$ is 300 K and $T_{\rm m}$ is 2023 K.[25] $a(0)$ is 4.5 nm and it is not depend on the specific ion energy E.[26] The efficiency g considerably varies with E in the range $0.17 < g < 0.5$ which is related to the velocity effect,[27] and g is 0.17 for the high ion velocities. So the calculated energy loss threshold of the track formation in MoS_2 is 9.7 keV/nm. Previously, Furuno *et al.*[28] observed the discrete tracks of 117 MeV Cl ions ($\sim$ 3 MeV/u) in MoS_2 at $(dE/dx)_e = 6.4$ keV/nm. It should be due to the velocity effect,[17,29] which has already been observed in other materials irradiated with swift heavy ions.[30–32] It is known that the radial distribution of δ electrons excited by incident ions in target materials is velocity-dependent. For high-velocity ion, the energy deposition is smeared out into a larger radius.

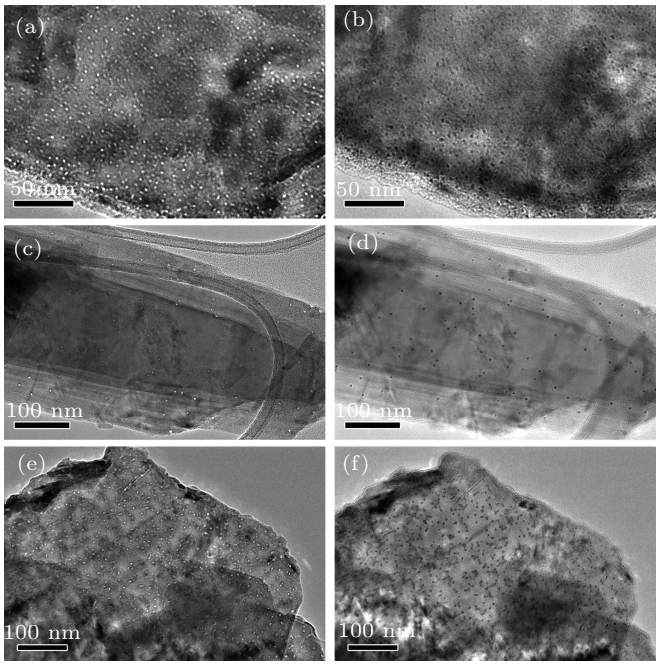

Fig. 2. Plan-view TEM images of MoS_2 after swift heavy ion irradiation with (a), (b) ^{129}Xe 5×10^{12} ions/cm^2, (c), (d) ^{181}Ta 5×10^{10} ions/cm^2, and (e), (f) ^{209}Bi 5×10^{11} ions/cm^2. The left and right rows are the phase contrast images obtained at under-focus and over-focus conditions, respectively.

The diameter distribution of ion tracks in irradiated MoS_2 with different $(dE/dx)_e$ is given in Fig. 3. It can be seen that the average diameter of ion tracks (D_a) increases from 1.9 nm to 4.5 nm as $(dE/dx)_e$ increases from 18.9 keV/nm to 35.2 keV/nm. It is consistent with the diameters of tracks created by 1 GeV Pb ions at $(dE/dx)_e = 36.0$ keV/nm.[33]

Although the Fresnel contrast of the tracks was observed in the irradiated samples under normal incidence, it needs to be validated further whether the track is partly or entirely empty. In order to observe the actual morphologies along the entire length of the ion track in MoS_2, the irradiation experiments under 30° incidence were carried out and the TEM results are shown in Fig. 4. The morphology of the entire track in Fig. 4(a) appears to be cylindrical with an apparent length about 30 nm. The circular features at each end of the tracks are visible and the diameter is about 4 nm. They can be assigned as spherical hillocks formed on the both surfaces of the sample.[17,21] According to the thermal spike model,[29] it is known that local melting occurs along the ion path during interacting with SHIs as sketched in Figs. 5(a) and 5(b). Due to the difference between the densities of matrix (solid) phase and molten (liquid) phase, the molten matter will flow out to the top and bottom surfaces to release the enhanced interior pressure. Then the hillocks are formed (Fig. 5(c)) and they adopt spherical shapes because the surface area and potential energy of the sphere are smallest. The whole formation process of ion tracks may take about 10–100 ps.[34] The formation of hillocks implies that there are some empty parts in the track, and it is consistent with the observed Fresnel contrasts in the plan view of TEM (Fig. 2). We also compared the volume of two hillocks (V_h) and track on the ion path (V_{tr}) in irradiated MoS_2. In the case of the track shown in Fig. 3(a), the V_h is 83.2 nm^3 which is significantly smaller than V_{tr} (435.4 nm^3). Thus, it can be speculated that the interior of the ion track in MoS_2 is not completely empty.

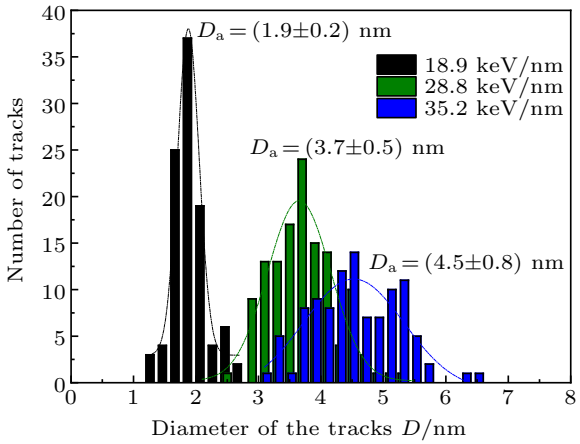

Fig. 3. Statistical diameter distribution of ion tracks in irradiated MoS_2 with different electronic energy losses. The average diameters of the ion tracks (D_a) are fitted according to Gaussian curve.

As the apparent length increases to about 180 nm, the ion track morphology displays a sandglass-like shape and the "waist" location is marked by the red arrow in Fig. 4(b). The cones of ion track appear next to the hillocks when the apparent length increases further and it looks like q-tips-like shape as shown in Fig. 4(c). Those special track morphologies attribute to the recrystallization process of the molten phase, which starts along the matrix-molten phase interface and has a similar lattice with initial states (Fig. 5(d)). Moreover, the tracks seem to be continuous with apparent length of longer

than 187 nm. The present results are different from our previous results in the case of rutile TiO_2, where the ion track was discontinuous for the ion path length longer than 150 nm.[17] The tracks are still continuous in irradiated MoS_2 when the ion path length (or actual track length) is even longer than 216 nm. The actual track length was estimated according to the simple relation between the apparent length (L_{ap}) and actual track length (L_{ac}), given by $L_{ac} = L_{ap}/\cos 30°$.

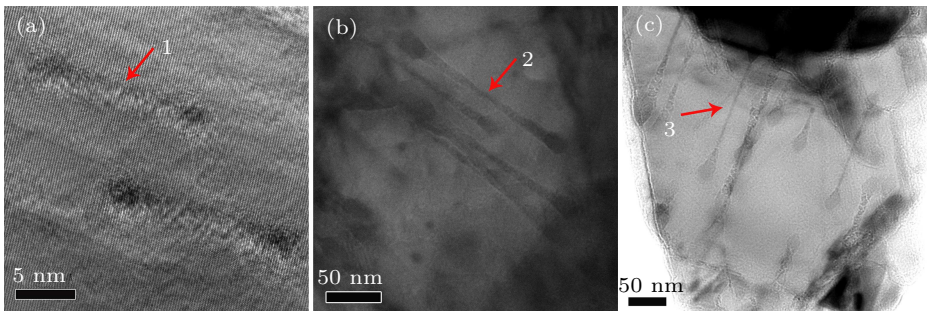

Fig. 4. TEM images of different ion track morphologies of MoS_2 irradiated at 30° with 1785.7 MeV ^{181}Ta ions. (a) Nearly cylindrical ion tracks consist of two spherical hillocks at each end. (b) Sandglass-like ion tracks. The apparent length in MoS_2 sample is about 180 nm. (c) The q-tips-like ion tracks. The size of hillocks increases with increasing apparent length.

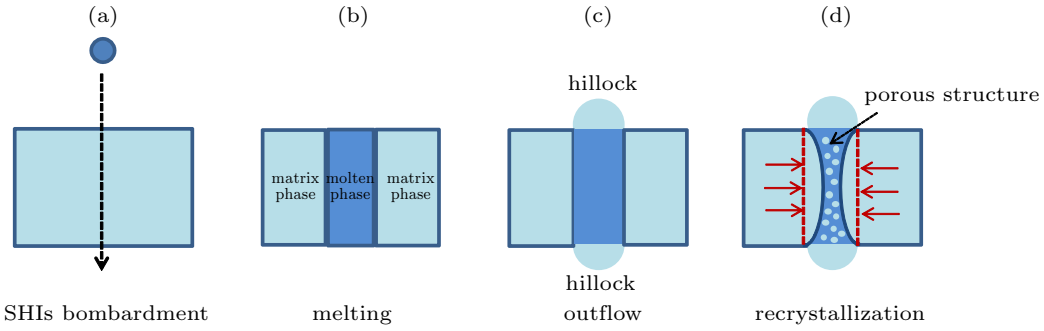

Fig. 5. Schematics of the formation process of ion track in irradiated MoS_2 with SHIs. (a) SHIs bombardment. (b) Target material melting along the ion path. (c) Outflow of molten phase towards the free surface. (d) Recrystallization in ion damage zone.

Table 2. Track related parameters of MoS_2 with different morphologies. Morphology, hillock diameter (D_h), apparent track length (L_{ap}), and actual track length (L_{ac}) were obtained from TEM measurements in Fig. 3.

Morphology	L_{ap}/nm	L_{ac}/nm	D_h/nm
cylinders	30.5 ± 1.0	35.2 ± 1.2	4.0 ± 0.2
sunglass	180.3 ± 1.1	208.2 ± 1.3	16.6 ± 0.7
q-tips	187.4 ± 1.4	216.4 ± 1.6	20.6 ± 1.1

Another remarkable feature is that these q-tips-like tracks have very big hillocks ($\sim$ 21 nm), which are five times as big as presented in Fig. 4(a). The related track data of MoS_2 with different morphologies are shown in Table 2. As a comparison, the hillocks in various morphologies of ion tracks almost have the same size in rutile TiO_2 and they do not change with the ion path length.[17] Thus, it can be deduced that the diameter of hillock and the morphology of ion tracks change as a function of the ion path length in irradiated MoS_2. Until now, similar morphologies of the ion tracks were also observed in several oxides such as rutile TiO_2, Al_2O_3, YSZ, and $Gd_2Zr_2O_7$ pyrochlore.[17–20] Here, it is the first time to observe various morphologies of ion tracks in non-oxides MoS_2, which has typical layered crystal structure and strong anisotropy.

In fact, the cylindrical tracks are more common and they were always observed in many irradiated materials, such as NiO,[22] zircon,[35] apatite,[36] and YIG.[37] During the formation of ion tracks, the recrystallization ability is a critical factor determining the track morphology,[17,38] which is considered to be related to the intrinsic properties of materials, such as the lattice structure and atomic diffusion velocity. The complexity of material structure can be considered as a crude estimate of the recrystallization ability in SHI tracks.[38] The simulation on atomic pair distribution function analysis found that MgO (3 peaks, cubic system) with "simple" lattice structure has strong recrystallization ability, so that the SHI tracks can be recovered to almost the virgin state. For comparison, partial recovery was found in Al_2O_3 (15 peaks, trigonal system) and almost no recovery in $Y_3Al_5O_{12}$ (YAG, 19 peaks, cubic system).[38] In other words, these "complex" lattice structures can suppress recrystallization. The lattice structure of MoS_2 has 5 peaks[39] in pair distribution function which are slightly more than those of MgO. Therefore, it can be predicted that the recrystallization ability of MoS_2 is poor than MgO but stronger than YAG. On the other hand, the earlier studies have revealed that the growth rate of high-energy facets in the lateral direction is higher than that of the low-energy facets in the vertical direction in naturally layered materials,[40,41] and the competition between the intralayer and interlayer interactions is the key factor for materials growth.[42] Therefore, the recrystallization growth of MoS_2 in molten zone

can be significantly different from those of oxides bulk materials, which is attributed to the layered structure and strong anisotropy. The evidence of recrystallization process in irradiated graphite with heavy ions was also found by using Raman spectroscopy.[43]

Now, we discuss the possible reason for the conical shape formation. The target material is transiently heated during interaction with SHIs and generates a molten area. Subsequently, thermal expansion causes a compressive stress in the material. The stress gradients propel the molten matter towards and out of the surfaces from the track interior.[22] The interior atoms which are farther from the surface in melting phase require more energy and time to flow out than those atoms closer to the upper and lower surfaces. The deeper atoms in melting phase can hardly move to the surface, and finally are left in materials. In this case, they are easier to preferentially recrystallize along the interface between the matrix and molten phases in terms of epitaxial growth. Thus, the formation of the conical shape tracks is attributed to the cooperation between the outflow of molten matter near the surface and the recrystallization during the rapid quenching.

4. Conclusion

The ion tracks in MoS_2 were created by electronic energy loss processes above a critical threshold of 9.7 keV/nm. Fresnel contrast was observed for ion tracks in MoS_2 by TEM which indicates the lower density in the ion track. The cylindrical, sandglass-like, and q-tips-like morphologies of ion tracks were observed in SHIs irradiated MoS_2 as a function of the ion path length. It was proposed that the recrystallization plays a major role in forming different morphologies of ion tracks, and the recrystallization ability seems to be related with the complexity of lattice structure in MoS_2.

Acknowledgment

We would like to thank the accelerator staff of the HIRFL and Dr. Khan Maaz for his improvement of the paper.

References

[1] Dufour Ch, Audouard A, Beneu F, Dural J, Girard J P, Hairie A, Levalois M, Paumier E and Toulemonde M 1993 *J. Phys.: Condens. Matter* **5** 4573
[2] Heiranian M, Farimani A B and Aluru N R 2015 *Nat. Commun.* **6** 8616
[3] Zollondz J H and Weidinger A 2004 *Nucl. Instrum. Methods Phys. Res. B* **225** 178
[4] Mara A, Siwy Z, Trautmann C, Wan J and Kamme F 2004 *Nano Lett.* **4** 497
[5] Fink D, Chadderton L T, Kiv A, Saad A, Tabacnics M, Rizutto M de A, Silva A de O D, Fahrner W R and Hoppe K 2007 *Radiat. Eff. Defects Solids* **162** 543
[6] Madauß L, Zegkinoglou I, Muiños H V, Choi Y W, Kunze S, Zhao M Q, Naylor C H, Ernst P, Pollmann E, Ochedowski O, Lebius H, Benyagoub A, Ban-d'Etat B, Johnson A T C, Djurabekova F, Cuenya B R and Schleberger M 2018 *Nanoscale* **10** 22908
[7] Liu J, Neumann R, Trautmann C and Müller C 2001 *Phys. Rev. B* **64** 184115
[8] Vazquez H, Åhlgren E H, Ochedowski O, Leino A A, Mirzayev R, Kozubek R, Lebius H, Karlusic M, Jaksic M, Krasheninnikov A V, Kotakoski J, Schleberger M, Nordlund K and Djurabekova F 2017 *Carbon* **114** 511
[9] Akcöltekin S, Bukowska H, Peters T, Osmani O, Monnet I, Alzaher I, Ban d'Etat B, Lebius H and Schleberger M 2011 *Appl. Phys. Lett.* **98** 103103
[10] Schleberger M and Kotakoski J 2018 *Materials* **11** 1885
[11] Madauß L, Ochedowski O, Lebius H, Ban-d'Etat B, Naylor C H, Johnson A T C, Kotakoski J and Schleberger M 2017 *2D Mater.* **4** 015034
[12] Radisavljevic B, Radenovic A, Brivio J, Giacometti V and Kis A 2011 *Nat. Nanotechnol.* **6** 147
[13] Bertolazzi S, Krasnozhon D and Kis A 2013 *ACS Nano* **7** 3246
[14] Hilton M R and Fleischauer P D 1992 *Surf. Coat. Technol.* **54–55** 435
[15] Kang Y M, Najmaei S, Liu Z, Bao Y J, Wang Y M, Zhu X, Halas N J, Nordlander P, Ajayan P M, Lou J and Fang Z Y 2014 *Adv. Mater.* **26** 6467
[16] Henry J, Dunlop A and Della-Negra S 1998 *Nucl. Instr. Meth. Phys. Res. Sect. B* **146** 405
[17] Zhai P F, Nan S, Xu L J, Li W X, Li Z Z, Hu P P, Zeng J, Zhang S X, Sun Y M and Liu J 2019 *Nucl. Instr. Meth. Phys. Res. Sect. B* **457** 72
[18] O'Connell J, Skuratov V, van Vuuren A J, Saifulin M and Akilbekov A 2016 *Phys. Status Solidi B* **253** 2144
[19] Garrido F, Moll S, Sattonnay G, Thomé L and Vincent L 2009 *Nucl. Instr. Meth. Phys. Res. Sect. B* **267** 1451
[20] Lang M, Toulemonde M, Zhang J, Zhang F, Tracy C L, Lian J, Wang Z, Weber W J, Severin D, Bender M, Trautmann C and Ewing R C 2014 *Nucl. Instr. Meth. Phys. Res. Sect. B* **336** 102
[21] Ishikawa N, Okubo N and Taguchi T 2015 *Nanotechnology* **26** 355701
[22] Schattat B, Bolse W, Klaumünzer S, Zizak I and Scholz R 2005 *Appl. Phys. Lett.* **87** 173110
[23] Cowley J, Moodie A 1960 *Proc. Phys. Soc. London* **76** 378
[24] Szenes G, Paszti F, Peter A and Popov A I 2000 *Nucl. Instr. Meth. Phys. Res. Sect. B* **166-167** 949
[25] Chase M W 1998 *Journal of Physical Chemical Reference Data*, Monograph No. 9 (New York: American Institute of Physics) p. 1594
[26] Szenes G 1995 *Phys. Rev. B* **51** 8026
[27] Szenes G 1999 *Phys. Rev. B* **60** 3140
[28] Furuno S, Otsu H, Hojou K and Izui K 1996 *Nucl. Instr. Meth. Phys. Res. Sect. B* **107** 223
[29] Toulemonde M, Assmann W, Dufour C, Meftah A, Studer F and Trautmann C 2006 *Symposium on Ion Beam Science - Solved and Unsolved Problems*, May 1–5, 2006, Copenhagen, Denmark, p. 263
[30] Meftah A, Brisard F, Costantini J, Hage-Ali M, Stoquert J, Studer F and Toulemonde M 1993 *Phys. Rev. B* **48** 920
[31] Zhai P F, Liu J, Duan J L, Chang H L, Zeng J, Hou M D, Sun Y M 2011 *Nucl. Instr. Meth. Phys. Res. Sect. B* **269** 2035
[32] Zhai P F, Liu J, Zeng J, Yao H J, Duan J L, Hou M D, Sun Y M and Ewing R 2014 *Chin. Phys. B* **23** 126105
[33] Henry J, Dunlop A, Della-Negra S and Chadderton L T 1997 *Rad. Meas.* **28** 71
[34] Trautmann C, Toulemonde M, Dufour C and Paumier E 1996 *Nucl. Instr. Meth. Phys. Res. Sect. B* **108** 94
[35] Li W, Kluth P, Schauries D, Rodriguez M, Lang M, Zhang F, Zdorovets M, Trautmann C and Ewing R C 2014 *Am. Mineral.* **99** 1127
[36] Li W, Lang M, Gleadow A J W, Zdorovets M V and Ewing R C 2012 *Earth Planet. Sci. Lett.* **321–322** 121
[37] Jensen J, Dunlop A, Della-Negra S and Pascard H 1998 *Nucl. Instr. Meth. Phys. Res. Sect. B* **135** 295
[38] Rymzhanov R A, Medvedev N, O'Connell J H, Janse van Vuuren A, Skuratov V A and Volkov A E 2019 *Sci. Rep.* **9** 3837
[39] Petkov V, Billinge S J L, Larson P, Mahanti S D, Vogt T, Rangan K K and Kanatzidis M G 2002 *Phys. Rev. B* **65** 092105
[40] Jang J T, Jeong S, Seo J W, Kim M C, Sim E, Oh Y, Nam S, Park B and Cheon J 2011 *J. Am. Chem. Soc.* **133** 7636
[41] Manna L, Wang L W, Cingolani R and Alivisatos A P 2005 *J. Phys. Chem. B* **109** 6183
[42] Xue X X, Feng Y X, Chen K Q and Zhang L X 2018 *J. Chem. Phys.* **148** 134704
[43] Zhai P F, Liu J, Zeng J, Duan J L, Xu L J, Yao H J, Guo H, Zhang S X, Hou M D and Sun Y M 2016 *Carbon* **101** 22